Observation of Efimov Universality across a Nonuniversal Feshbach Resonance in ^{39}K

Xin Xie,[1] Michael J. Van de Graaff,[1] Roman Chapurin,[1] Matthew D. Frye,[2] Jeremy M. Hutson,[2] José P. D'Incao,[1] Paul S. Julienne,[3] Jun Ye,[1] and Eric A. Cornell[1]

[1]*JILA, National Institute of Standards and Technology and the University of Colorado, and Department of Physics, Boulder, Colorado 80309, USA*

[2]*Joint Quantum Centre (JQC) Durham-Newcastle, Department of Chemistry, Durham University, South Road, Durham DH1 3LE, United Kingdom*

[3]*Joint Quantum Institute, National Institute of Standards and Technology and the University of Maryland, College Park, Maryland 20742, USA*

(Received 22 July 2020; accepted 19 October 2020; published 7 December 2020)

We study three-atom inelastic scattering in ultracold ^{39}K near a Feshbach resonance of intermediate coupling strength. The nonuniversal character of such resonance leads to an abnormally large Efimov absolute length scale and a relatively small effective range r_e, allowing the features of the ^{39}K Efimov spectrum to be better isolated from the short-range physics. Meticulous characterization of and correction for finite-temperature effects ensure high accuracy on the measurements of these features at large-magnitude scattering lengths. For a single Feshbach resonance, we unambiguously locate four distinct features in the Efimov structure. Three of these features form ratios that obey the Efimov universal scaling to within 10%, while the fourth feature, occurring at a value of scattering length closest to r_e, instead deviates from the universal value.

DOI: 10.1103/PhysRevLett.125.243401

Physics has always been about explaining a lot with a little. From single-particle harmonic oscillators to critical exponents in many-body physics, we look for parsimonious descriptions and simple patterns that are universal over a huge range of energy and length scales, independent of the details of the system. The motion of three bodies, especially when of comparable masses, is famously unamenable to the application of such universal ideas. A dramatic exception occurs when the system is characterized by pairwise interactions which are near resonant, i.e., with the s-wave scattering length a large compared to the range of the pairwise physical potential. This is the realm of Efimov physics [1–4].

Three identical [5] bosons have been shown theoretically to support an infinite sequence of three-body bound states, the Efimov states, whose spectrum as a function of a displays discrete scaling invariance [1,2]. The lovely recursive pattern of energy levels and associated log-periodic structure of three-body observables—inelastic collision rates—are depicted schematically in Fig. 1. Features in the spectrum associated with successive generations of Efimov states form ratios of 22.7, while features on opposite sides of the resonance occur at a ratio of either -1.000 or -1.065 [2,4,17,18]. In the ideal case, these universal ratios identify the location of every feature up to a single absolute length scale. Experimental observation of this universal structure of Efimovian scaling has been a challenge, with relevant earlier measurements reviewed in the discussion near the end of this Letter. As for the absolute length scale, it was originally relegated to the status of species-dependent nonuniversal details [19]. Later it was empirically [20,21] and then theoretically [22–25] shown that in ultracold atom systems the absolute scale, as specified by the actual value of $a_-^{(0)}$, is often within 15% of $-9.7\,r_{\mathrm{vdW}}$, where r_{vdW} is the van der Waals length [26]. This "van der Waals universality" is by itself remarkable, but does not speak to the original notion of Efimov universality, which is about the *relative* location of multiple three-body features near a given two-body resonance.

What makes observations of the originally conceived Efimov universality [1,2] so difficult is a sandwiching effect. Universality assumes that a is tuned by an idealized zero-range two-body resonance, whereas any realistic scattering process is parameterized by an effective range r_e [27], the lowest-order correction to the zero-range approximation. Efimov features that appear at those values of a (yellow shaded zone in Fig. 1) that are so small as to be not well separated from r_e can be perturbed by short-range details. On the other hand, if a is too large (purple shaded zone in Fig. 1), finite-temperature and finite-density effects in a bulk gas will obscure the features. Counterintuitively, van der Waals universality is the enemy of Efimov universality. The "universal" value of $a_-^{(0)}$ in principle arises from strong Feshbach resonances and is relatively small in magnitude [22,23,25,28]. A strong resonance moreover gives rise to a large value of $r_e \approx 2.8 r_{\mathrm{vdW}}$ [29,30], causing experimentally accessible features in the Efimov spectrum to be perilously close to the yellow zone.

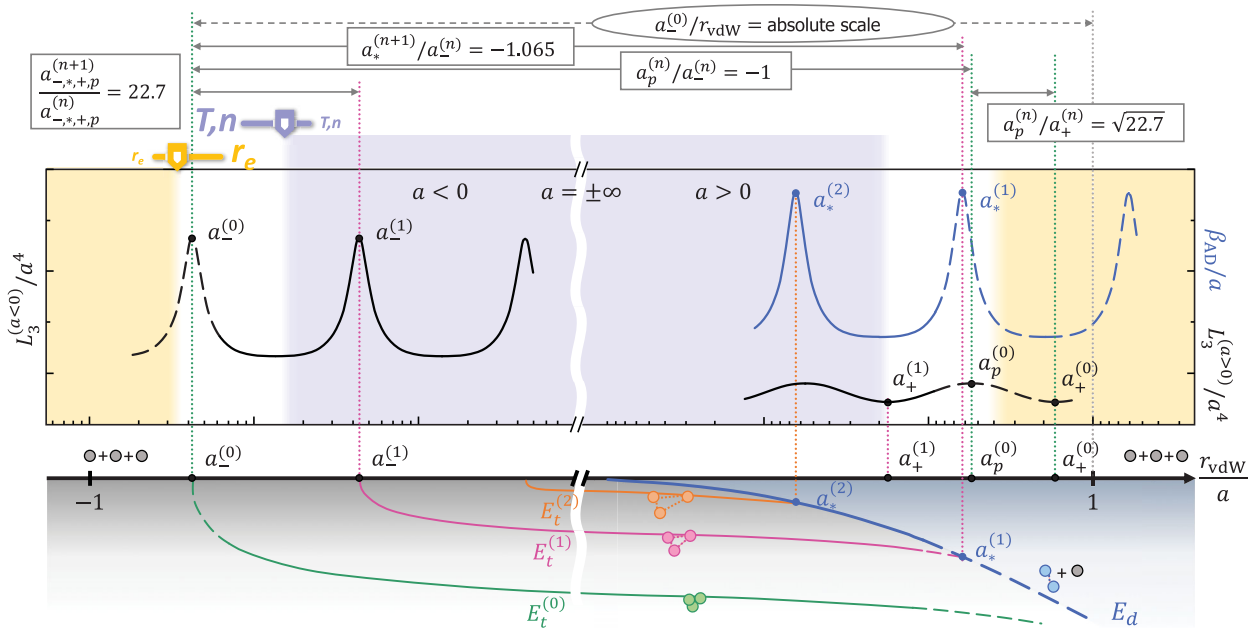

FIG. 1. Efimov universality. The bottom panel shows trimer ($E_t^{(n)}$) and dimer (E_d) energies as a function of a^{-1}, with energy levels distorted to make clearer the resonance locations. The nth trimer is resonant with three free atoms at $a = a_-^{(n)}$, and with the dimer at $a = a_*^{(n)}$. The middle panel depicts the rate coefficients for inelastic collisions. The three-body recombination coefficient L_3 peaks at each value of $a_-^{(n)}$, while the atom-dimer relaxation coefficient $\beta_{\rm AD}$ peaks at each value of $a_*^{(n)}$. The entire structure is log-periodic with period 22.7. For $a > 0$, L_3/a^4 shows quantum interference, with each local maximum $a_p^{(n)}$ spaced from the corresponding local minimum $a_+^{(n)}$ by $\sqrt{22.7}$. Each value of $a_p^{(n)}$ is related to the corresponding $a_-^{(n)}$ by a factor of exactly -1, but is offset from the nearest value of a_* by 6.5%. Going from relative to absolute values of a requires a single absolute scale indicated by the oval circle. All these ratios are for the zero-range limit; the dashed curves suggest the possibility of perturbations as $|a|$ enters the region, indicated by yellow shading, where it is not large compared to the effective range r_e. The range of the yellow zone may be "adjusted" by choosing atomic species with different r_e. The purple shading represents regions of large $|a|$ that are prone to systematic effects such as those caused by finite temperature and density.

In this Letter, we instead work with an intermediate-strength Feshbach resonance in ^{39}K, centered at 33.5820 (14) G and with width 54.772 G [31]. Too weak to obey van der Waals universality, our resonance gives rise to a correspondingly smaller r_e, and a larger magnitude $a_-^{(0)}$ [31]. The Efimov features hence tend to occur at higher values of $|a|/r_e$, away from the yellow zone. We have carefully characterized four distinct triatomic Efimov features associated with a single Feshbach resonance, an unprecedented achievement. For each measured feature, we study the temperature dependence of its location in order to extract a $T \to 0$ value, thus minimizing the hazard represented by the purple zone. These four locations yield three independent ratios which give a measure of redundancy (see Fig. 1). We identify three of these features which are arranged in Efimov universal ratios and one (the one at the lowest value of $|a|$) which is distinctly nonuniversal. Further confidence in our experimental observables comes from excellent agreement with our theoretical analysis, performed using a complete two-body coupled-channel model and a realistic three-body model built upon hyperspherical adiabatic representation, which incorporates the proper hyperfine structure and a variable number of singlet and triplet two-body bound states [31–33].

The Efimov feature for $a < 0$ (the triatomic resonance) was studied in our previous work [31]. Here, for $a > 0$, we first discuss the atom-dimer scattering resonance, which manifests as enhanced atom-dimer inelastic decay rate, $\beta_{\rm AD}$. After the evaporative cooling in a pancake-shaped crossed dipole trap, we end up with a spin-polarized cloud at various temperatures. An admixture of atoms and dimers is generated by magnetoassociation of the dimers and followed by a step to precisely control the atom density. We then hold the samples at different magnetic fields and track the populations of the dimers as they either break apart on their own or react with free atoms. The dimers in nonground Zeeman sublevels are known to dissociate spontaneously and spin flip into d-wave exit channels [44,45]. This decay process contributes to a background loss of dimers as shown in Fig. 2(a). The pure dimer lifetime shows a peak around $a = 65a_0$. We calculate this lifetime using coupled-channel methods [46–48] and find that the position and height of the peak are very sensitive to interference between different d-wave decay paths.

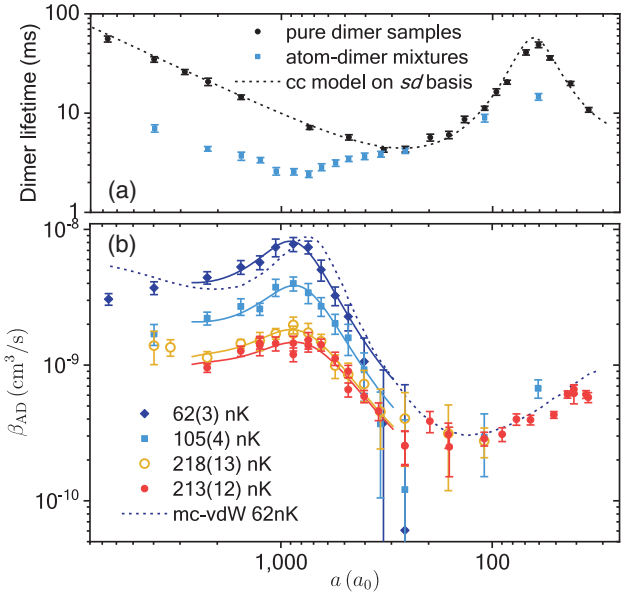

FIG. 2. Temperature dependence of atom-dimer relaxation coefficient β_{AD} as a function of a. (a) Lifetimes of dimers with and without atoms being present. The black circles represent the intrinsic lifetimes of the dimers measured on dimer samples with $\langle n_D \rangle = 2 \times 10^9$ cm^{-3}, $T = 70$ nK. Error bars are extracted from the fitting routine and include only the statistical noise on dimer number. The dashed line represents a coupled-channel model that includes spin-spin dipolar interaction plus second-order spin-orbit coupling [33]. (b) β_{AD} measured at various temperatures. Atomic densities differ by a factor of 3 between the two highest temperature datasets. Error bars stand for 1σ propagated uncertainty involving the statistical error of atom density as well as the uncertainty of dimer lifetimes. Solid lines are fitting curves with a finite-temperature model [50]. The navy dashed line is an independent prediction of our three-body multichannel (MC-vdW) model with no adjustable parameters at 62 nK, obtained using 4 (3) s-wave singlet (triplet) two-body bound states [33].

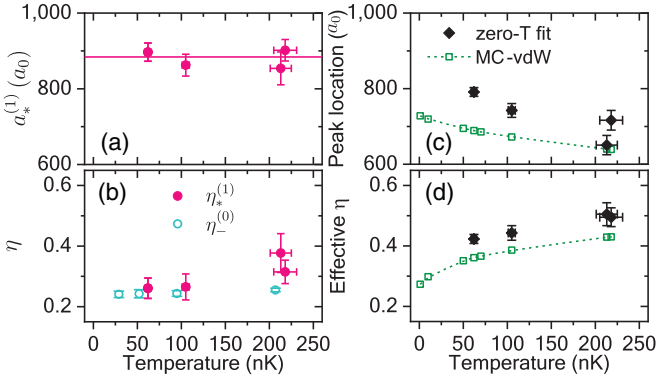

FIG. 3. Summary of the fit results on atom-dimer resonance and comparison with MC-vdW theory. (a) $a_*^{(1)}$ and (b) $\eta_*^{(1)}$ extracted from the finite-temperature model fits (magenta circles). The horizontal line indicates the mean value of the four points. $\eta_*^{(1)}$ is found to be consistent with $\eta_-^{(0)}$ reported in our previous work [31]. (c) Phenomenological peak location and (d) inelasticity extracted from the zero-temperature fits to the finite-temperature data (black diamonds) or model (green squares). Finite-temperature effects not only shift the peak location but also greatly broaden the peaks. Both behaviors are captured by our MC-vdW model.

We determine the strength of the second-order spin-orbit coupling, which was previously neglected [49] but significantly influences the balance between paths here [33]. The dashed line in Fig. 2(a) shows the resulting theoretical curve. On top of this two-body inelastic process, we observe that the dimers become shorter lived due to their reaction with atoms. By subtracting out the dimer one-body decay rate from the dimer total decay rate [33], we extract the atom-dimer relaxation coefficient β_{AD} at different temperatures as plotted in Fig. 2(b). A resonant peak is pronounced at all temperatures. The highest-temperature data were collected with multiple atom densities in order to verify the negligible role of four-body processes.

To quantitatively study the resonant behavior of β_{AD}, we fit the data [Fig. 2(b)] with a zero-range effective-field theory [50] that provides a convenient parametrization of atom-dimer scattering at finite energy. There are two free parameters in this model, a_* and η_* [33]. a_* denotes the position of the resonance where an Efimov state merges into the atom-dimer scattering threshold; η_* is the inelasticity parameter that characterizes the probability of decay into an energetic atom and deep dimer. We include an additional parameter in the fitting function, the global magnitude A_*, which serves as a diagnostic indicator of the overall consistency between experiment and theory. The temperature of the sample, which is an input parameter to this model, is measured with absorption images on atoms after a long time of flight. As depicted by the set of solid lines, this finite-temperature model captures the shape of the atom-dimer resonance peak across the whole temperature range accessed in our experiment.

The variation of the fitting parameters with temperature is summarized in Fig. 3. We contrast the fit results from the above-mentioned finite-temperature model [51] [panel (a) and (b)] and from a zero-temperature model [2] [panel (c) and (d)]. The former model reveals an energy-independent parameter $a_*^{(1)}$ that is approached by the phenomenological peak location from the latter model as $T \to 0$. We determine $a_*^{(1)} = 884(14)a_0 = 13.7(2)r_{vdW}$ from the weighted mean of the four experimental points [Fig. 3(a)]. Notably, the inelasticity parameter $\eta_*^{(1)} = 0.28(2)$ overlaps with the previously measured $\eta_-^{(0)} = 0.25(1)$ for $a < 0$ within uncertainty [Fig. 3(b)], indicating that the same parameter characterizes Efimov states on both sides of the two-body resonance.

We determine the remaining two Efimov features for $a > 0$ through measurements of three-body recombination coefficient L_3. Unlike for $a < 0$, there are no expected three-body resonances in L_3 for $a > 0$. Instead, two

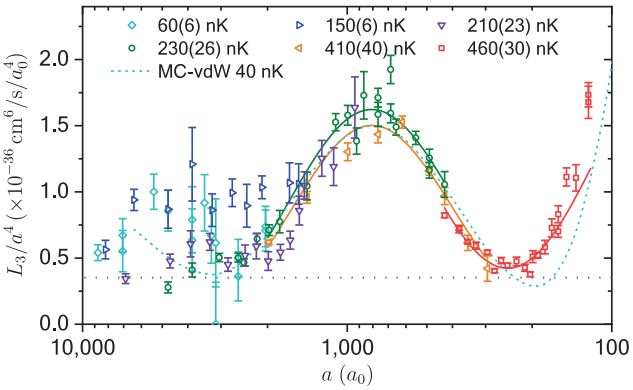

FIG. 4. Three-body recombination coefficient L_3 divided by a^4 as a function of a. Colored solid lines represent fits to a finite-temperature model in the neighborhood of either the maximum or the minimum. The dotted horizontal line represents three-body recombination into deeply bound dimers with $\eta_+^{(0)} = 0.20$. The cyan dashed line represents our MC-vdW calculation done for 40 nK [33].

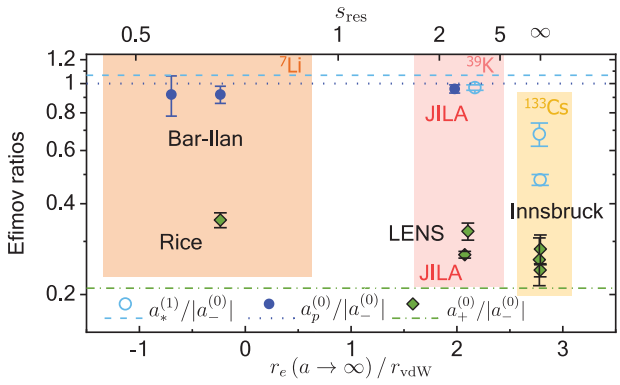

FIG. 5. Summary of experimental [20,31,53–58,62] and theoretical results [4] of three Efimov ratios between features on opposite sides of the Feshbach resonance. Here we show only the experiments on the observables presented in Fig. 1. The two JILA points at the top are artificially spaced in horizontal direction for visibility. The corresponding zero-range theory predictions are shown as the dashed, dotted and dash-dotted lines. r_e is evaluated at unitarity ($a \to \infty$) using the model given in [31], in which r_e is related to the coupling-strength parameter s_{res} [26,31] that defines strong ($s_{\mathrm{res}} \gg 1$) and weak ($s_{\mathrm{res}} \ll 1$) Feshbach resonances.

indistinguishable decay pathways lead to interference minima and maxima [2–4], denoted as $a_+^{(n)}$ and $a_p^{(n)}$, respectively. Upon finishing the evaporation, we ramp up the trap depth adiabatically to about 10 times the final temperature to avoid number loss due to ongoing evaporation. The peak value of the phase-space density is always restricted below 1 to ensure Boltzmann statistics. We use a rate equation [33] to describe the time evolution of atom number and temperature to obtain the value of L_3 at various a. Since the overall scaling of L_3 is proportional to a^4, we divide out this prefactor in Fig. 4 to emphasize the log-periodic modulation due to Efimov physics.

To extract the minimum $a_+^{(0)}$, we fit the dataset of 460 nK with the finite-temperature model [52] (red solid line in Fig. 4). There are three free parameters in our fitting function, a_+ and η_+ accounting for the location of the minimum and the contrast of the oscillation, and an amplitude-scaling factor A_+. We obtain $a_+^{(0)} = 246(6)a_0$, $\eta_+^{(0)} = 0.20(2)$. This result agrees with a fit with a zero-range, zero-energy model [2], suggesting the negligible effects of finite temperature on $a_+^{(0)}$. To extract the maximum $a_p^{(0)}$, we fix the contrast parameter to 0.20 in the same finite-temperature model and fit the datasets of 410 nK and 230 nK with the empirical temperatures as inputs. We determine $a_p^{(0)} = 876(28)a_0$ from the mean value of the two conditions. For fits at all three temperatures, the mean value of A_+ is within 17% of unity [33], consistent with our density calibration uncertainty of $<10\%$. As we scan a to larger values, poorly understood temperature and density effects complicate the interpretation of our L_3 measurements [33].

Discussion.—We compare our results on Efimov ratios with previous experimental work [5] in Fig. 5. The particular ratio $a_*^{(1)}/a_-^{(0)}$ substantially deviates from the zero-range universal value when r_e is large and positive. This is the case for strong Feshbach resonances such as those used in ^{133}Cs [53]. For our intermediate-strength resonance in ^{39}K, with suppressed r_e and $a_-^{(0)} = -14.05(17)\,r_{\mathrm{vdW}}$ [31], we obtain $a_*^{(1)}/a_-^{(0)} = -0.97(2)$. This is within 9% of the universal ratio of -1.065 [17]. The much better agreement makes sense in light of the greater separation of length scales. Quantitatively, $|a_-^{(0)}|$ and $a_*^{(1)}$ are only about 2 to 3 times r_e for ^{133}Cs, whereas they are about 7 times r_e for ^{39}K. Similarly, our observed $a_p^{(0)}$ value is also well spaced from r_e, and we observe $a_p^{(0)}/a_-^{(0)}$ within 4% of its universal value of -1 [18]. The other two reported $a_p^{(0)}$ values were measured in ^{7}Li resonances with $r_e \approx 0$ [54,55]. Their ratios $a_p^{(0)}/a_-^{(0)} = -0.92(14)$ and $-0.92(6)$, although of lower precision, are also consistent with Efimov universality. Finally, Efimov universality yields $a_+^{(0)}/a_-^{(0)} = -1/\sqrt{22.7} = -0.210$. Empirical values of $a_+^{(0)}/a_-^{(0)}$ in ^{7}Li [56], ^{133}Cs [20,57,58], earlier work in ^{39}K [59], and our own ^{39}K result differ from this prediction by between 15% and 70%. Moreover, there is no trend towards improved agreement with lower $|r_e|$. We note that the value of r_e at such small a can differ significantly from the value of r_e at $a \to \infty$ [60], and in these circumstances the short-range effects must be analyzed on a case-by-case basis. Not reviewed in Fig. 5 is a measurement [61] of $a_-^{(1)}/a_-^{(0)}$ in ^{133}Cs, which was consistent with Efimov universality.

Finally, we compare our experimental results with various theoretical models in Table I. The central results of this Letter are the excellent three-way agreement

TABLE I. Summary of three-body benchmark features characterizing an Efimov spectrum in ^{39}K. The features for $a < 0$ and $a > 0$ are on opposite sides of the same Feshbach resonance. The locations of the features and their ratios are compared to various theoretical models. Efimov universality is a zero-range theory that defines the universal scaling of the Efimov structure but leaves undetermined the absolute locations of the various features. vdW (van der Waals) universality treats interactions with a single-channel vdW potential. The model pins down the absolute scale of the structure, and quantifies how low-lying Efimov states can be distorted by the vdW interactions. Multichannel vdW (MC-vdW), elaborated in Ref. [33], is our attempt at a more realistic theoretical model for our ^{39}K resonance.

Model	Observables for $a < 0$		Observables for $a > 0$					Efimov ratios		
	$a_-^{(0)}/a_0$	$\eta_-^{(0)}$	$a_*^{(1)}/a_0$	$\eta_*^{(1)}$	$a_+^{(0)}/a_0$	$\eta_+^{(0)}$	$a_p^{(0)}$	$a_*^{(1)}/\lvert a_-^{(0)}\rvert$	$a_+^{(0)}/\lvert a_-^{(0)}\rvert$	$a_p^{(0)}/\lvert a_-^{(0)}\rvert$
Efimov universality [4]	⋯	⋯	⋯	⋯	⋯	⋯	⋯	1.06522	0.209914	1
vdW universality [63]	−626	⋯	213	⋯	90	⋯	⋯	0.340	0.143	⋯
MC-vdW	−846(19)	0.21(1) [31]	809(1)	0.27(3)	200(1)	0.10(1)	817(1)	0.95(2)	0.236(5)	0.96(2)
Experimental	−908(11)	0.25(1) [31]	884(14)	0.28(2)	246(6)	0.20(2)	876(28)	0.97(2)	0.271(7)	0.96(3)

between the Efimov universality, MC-vdW and experimental values for the ratios $a_*^{(1)}/a_-^{(0)}$ and $a_p^{(0)}/a_-^{(0)}$, and the corresponding disagreement with the predictions of van der Waals universality.

In summary, we have tested Efimov universality in unprecedented detail and found that it holds remarkably well, even for a resonance that deviates substantially from van der Waals universality.

The authors thank J. Bohn, D. Petrov, D. Kang, W. Zwerger, and R. Schmidt for useful discussions. This work is supported by NSF Phys-1734006, NASA/JPL 1502690, Marsico Research Chair, NIST, and the U.K. Engineering and Physical Sciences Research Council (EPSRC) Grant No. EP/P01058X/1.

[1] V. Efimov, Phys. Lett. **33B**, 563 (1970).
[2] E. Braaten and H.-W. Hammer, Phys. Rep. **428**, 259 (2006).
[3] C. H. Greene, P. Giannakeas, and J. Pérez-Ríos, Rev. Mod. Phys. **89**, 035006 (2017).
[4] J. P. D'Incao, J. Phys. B **51**, 043001 (2018).
[5] Considerable experimental [6–12] and theoretical [13–16] work has explored Efimov universality in systems with unequal atomic masses or distinguishable spin states, but to keep the complexity of this Letter manageable, we do not review that fascinating topic here.
[6] G. Barontini, C. Weber, F. Rabatti, J. Catani, G. Thalhammer, M. Inguscio, and F. Minardi, Phys. Rev. Lett. **103**, 043201 (2009).
[7] J. R. Williams, E. L. Hazlett, J. H. Huckans, R. W. Stites, Y. Zhang, and K. M. O'Hara, Phys. Rev. Lett. **103**, 130404 (2009).
[8] T. Lompe, T. B. Ottenstein, F. Serwane, A. N. Wenz, G. Zürn, and S. Jochim, Science **330**, 940 (2010).
[9] R. S. Bloom, M.-G. Hu, T. D. Cumby, and D. S. Jin, Phys. Rev. Lett. **111**, 105301 (2013).
[10] R. Pires, J. Ulmanis, S. Häfner, M. Repp, A. Arias, E. D. Kuhnle, and M. Weidemüller, Phys. Rev. Lett. **112**, 250404 (2014).
[11] R. A. W. Maier, M. Eisele, E. Tiemann, and C. Zimmermann, Phys. Rev. Lett. **115**, 043201 (2015).
[12] J. Johansen, B. DeSalvo, K. Patel, and C. Chin, Nat. Phys. **13**, 731 (2017).
[13] Y. Wang, J. Wang, J. P. D'Incao, and C. H. Greene, Phys. Rev. Lett. **109**, 243201 (2012).
[14] J. Ulmanis, S. Häfner, R. Pires, E. D. Kuhnle, Y. Wang, C. H. Greene, and M. Weidemüller, Phys. Rev. Lett. **117**, 153201 (2016).
[15] Y. Wang, J. P. D'Incao, and B. D. Esry, in *Advances in Atomic, Molecular, and Optical Physics*, Vol. 62, edited by E. Arimondo, P. R. Berman, and C. C. Lin (Academic Press, New York, 2013), pp. 1–115.
[16] K. Helfrich and H. Hammer, J. Phys. B **44**, 215301 (2011).
[17] A. O. Gogolin, C. Mora, and R. Egger, Phys. Rev. Lett. **100**, 140404 (2008).
[18] K. Helfrich, H.-W. Hammer, and D. S. Petrov, Phys. Rev. A **81**, 042715 (2010).
[19] J. P. D'Incao, C. H. Greene, and B. D. Esry, J. Phys. B **42**, 044016 (2009).
[20] M. Berninger, A. Zenesini, B. Huang, W. Harm, H.-C. Nägerl, F. Ferlaino, R. Grimm, P. S. Julienne, and J. M. Hutson, Phys. Rev. Lett. **107**, 120401 (2011).
[21] R. J. Wild, P. Makotyn, J. M. Pino, E. A. Cornell, and D. S. Jin, Phys. Rev. Lett. **108**, 145305 (2012).
[22] J. Wang, J. P. D'Incao, B. D. Esry, and C. H. Greene, Phys. Rev. Lett. **108**, 263001 (2012).
[23] R. Schmidt, S. Rath, and W. Zwerger, Eur. Phys. J. B **85**, 386 (2012).
[24] P. Naidon, S. Endo, and M. Ueda, Phys. Rev. Lett. **112**, 105301 (2014).
[25] C. Langmack, R. Schmidt, and W. Zwerger, Phys. Rev. A **97**, 033623 (2018).
[26] C. Chin, R. Grimm, P. Julienne, and E. Tiesinga, Rev. Mod. Phys. **82**, 1225 (2010).
[27] J. R. Taylor, *Scattering Theory* (John Wiley and Sons, New York, 1972).
[28] C. Chin, arXiv:1111.1484.
[29] B. Gao, Phys. Rev. A **58**, 1728 (1998).
[30] B. Gao, Phys. Rev. A **84**, 022706 (2011).
[31] R. Chapurin, X. Xie, M. J. Van de Graaff, J. S. Popowski, J. P. D'Incao, P. S. Julienne, J. Ye, and E. A. Cornell, Phys. Rev. Lett. **123**, 233402 (2019).

[32] J. Wang, J. P. D'Incao, and C. H. Greene, Phys. Rev. A **84**, 052721 (2011).
[33] See Supplemental Material at http://link.aps.org/supplemental/10.1103/PhysRevLett.125.243401 for details of our experimental and theoretical methods, which includes Refs. [34–43].
[34] S. Falke, H. Knöckel, J. Friebe, M. Riedmann, E. Tiemann, and C. Lisdat, Phys. Rev. A **78**, 012503 (2008).
[35] M. Berninger, A. Zenesini, B. Huang, W. Harm, H.-C. Nägerl, F. Ferlaino, R. Grimm, P. S. Julienne, and J. M. Hutson, Phys. Rev. A **87**, 032517 (2013).
[36] F. H. Mies, C. J. Williams, P. S. Julienne, and M. Krauss, J. Res. Natl. Instit. Stand. Technol. **101**, 521 (1996).
[37] C. Strauss, T. Takekoshi, F. Lang, K. Winkler, R. Grimm, J. H. Denschlag, and E. Tiemann, Phys. Rev. A **82**, 052514 (2010).
[38] H. Suno, B. D. Esry, C. H. Greene, and J. P. Burke, Phys. Rev. A **65**, 042725 (2002).
[39] S. Jonsell, J. Phys. B **37**, S245 (2004).
[40] J. P. D'Incao, B. D. Esry, and C. H. Greene, Phys. Rev. A **77**, 052709 (2008).
[41] X. Xie, Precise calibrations of few-body physics in Potassium-39: Experiment and theory, Ph.D. thesis, University of Colorado Boulder, Boulder, 2020.
[42] C. Langmack, D. H. Smith, and E. Braaten, Phys. Rev. A **87**, 023620 (2013).
[43] B. S. Rem, A. T. Grier, I. Ferrier-Barbut, U. Eismann, T. Langen, N. Navon, L. Khaykovich, F. Werner, D. S. Petrov, F. Chevy, and C. Salomon, Phys. Rev. Lett. **110**, 163202 (2013).
[44] S. T. Thompson, E. Hodby, and C. E. Wieman, Phys. Rev. Lett. **94**, 020401 (2005).
[45] T. Köhler, E. Tiesinga, and P. S. Julienne, Phys. Rev. Lett. **94**, 020402 (2005).
[46] J. M. Hutson and C. R. Le Sueur, Comput. Phys. Commun. **241**, 9 (2019).
[47] J. M. Hutson and C. R. Le Sueur, MOLSCAT, BOUND and FIELD, version 2020.0", https://github.com/molscat/molscat (2020).
[48] M. D. Frye and J. M. Hutson, Phys. Rev. Research **2**, 013291 (2020).
[49] S. Falke, H. Knöckel, J. Friebe, M. Riedmann, E. Tiemann, and C. Lisdat, Phys. Rev. A **78**, 012503 (2008).
[50] K. Helfrich and H.-W. Hammer, Europhys. Lett. **86**, 53003 (2009).
[51] E. Braaten and H.-W. Hammer, Phys. Rev. A **70**, 042706 (2004).
[52] E. Braaten, H.-W. Hammer, D. Kang, and L. Platter, Phys. Rev. A **78**, 043605 (2008).
[53] A. Zenesini, B. Huang, M. Berninger, H.-C. Nägerl, F. Ferlaino, and R. Grimm, Phys. Rev. A **90**, 022704 (2014).
[54] N. Gross, Z. Shotan, S. Kokkelmans, and L. Khaykovich, Phys. Rev. Lett. **103**, 163202 (2009).
[55] N. Gross, Z. Shotan, S. Kokkelmans, and L. Khaykovich, Phys. Rev. Lett. **105**, 103203 (2010).
[56] P. Dyke, S. E. Pollack, and R. G. Hulet, Phys. Rev. A **88**, 023625 (2013).
[57] T. Kraemer, M. Mark, P. Waldburger, J. G. Danzl, C. Chin, B. Engeser, A. D. Lange, K. Pilch, A. Jaakkola, H.-C. Nägerl, and R. Grimm, Nature (London) **440**, 315 (2006).
[58] F. Ferlaino, A. Zenesini, M. Berninger, B. Huang, H.-C. Nägerl, and R. Grimm, Few-Body Syst. **51**, 113 (2011).
[59] S. Roy, M. Landini, A. Trenkwalder, G. Semeghini, G. Spagnolli, A. Simoni, M. Fattori, M. Inguscio, and G. Modugno, Phys. Rev. Lett. **111**, 053202 (2013).
[60] C. L. Blackley, P. S. Julienne, and J. M. Hutson, Phys. Rev. A **89**, 042701 (2014).
[61] B. Huang, L. A. Sidorenkov, R. Grimm, and J. M. Hutson, Phys. Rev. Lett. **112**, 190401 (2014).
[62] M. Zaccanti, B. Deissler, C. D'Errico, M. Fattori, M. Jona-Lasinio, S. Müller, G. Roati, M. Inguscio, and G. Modugno, Nat. Phys. **5**, 586 (2009).
[63] P. M. A. Mestrom, J. Wang, C. H. Greene, and J. P. D'Incao, Phys. Rev. A **95**, 032707 (2017).